Available online at www.sciencedirect.com
ScienceDirect
Journal of Bionic Engineering 7 (2010) 56–65

Fuzzy Vorticity Control of a Biomimetic Robotic Fish Using a Flapping Lunate Tail

Tianmiao Wang[1], Li Wen[1], Jianhong Liang[1], Guanhao Wu[2]

1. *Robotic Institute*, *School of Mechanical Engineering and Automation*, *Beihang Unviversity*, *Beijing* 100191, *P. R. China*
2. *State Key Laboratory of Precision Measurement*, *Technology and Instruments*, *Department of Precision Instruments*, *Tsinghua University*, *Beijing* 100084, *P. R. China*

Abstract

Vorticity control mechanisms for flapping foils play a guiding role in both biomimetic thrust research and modeling the forward locomotion of animals with wings, fins, or tails. In this paper, a thrust-producing flapping lunate tail is studied through force and power measurements in a water channel. Proper vorticity control methods for flapping tails are discussed based on the vorticity control parameters: the dimensionless transverse amplitude, Strouhal number, angle of attack, and phase angle. Field tests are conducted on a free-swimming biomimetic robotic fish that uses a flapping tail. The results show that active control of Strouhal number using fuzzy logic control methods can efficiently reduce power consumption of the robotic fish and high swimming speeds can be obtained. A maximum speed of 1.17 length specific speed is obtained experimentally under conditions of optimal vorticity control. The *St* of the flapping tail is controlled within the range of 0.4~0.5.

Keywords: flapping tail, vorticity control, biomimetic robotic fish, fuzzy logic control

doi: 10.1016/S1672-6529(09)60183-9

1 Introduction

The thrust efficiency of fish can reach up to 80%. Aquatic animals with lunate tails, such as tuna, dolphin, or whale, can achieve a maximum swimming speed of 20 knots. These animals keep their bodies rigid while swimming, and the flapping lunate tail forms an efficient thruster, resembling a flapping foil. Two-dimensional (2D) flapping foil theory played a guiding role in biomimetic fish-like propulsion, which has been studied using hydrodynamic experiments[1]. The high-lift mechanisms of birds and insects, and locomotion via caudal fins and pectoral fins, have been modeled by oscillating foils[2]. The Strouhal number (*St*) is closely related to the thrust coefficient and thrust efficiency (or the lift force in a flight mechanism). Triantafyllou[3] used *St* to describe the vortex shedding of a fish's flapping tail fin, and found that the optimal combination of thrust coefficient and thrust efficiency was generated in the range of $0.2<St<0.4$. The optimal *St* of insect and bird flight is also in this range. When it is low ($St<0.05$), the flapping foil will be unable to provide sufficient thrust, and may even generate negative force. Conversely, when the *St* is high ($St > 0.6$), the thrust efficiency will be lower than the optimal range, even though a large thrust coefficient will be generated[4].

In addition to *St*, other parameters that can influence the thrust performance of an oscillating foil (the so-called "vorticity control parameters") are the maximum angle of attack, α_{max}, the dimensionless heave amplitude, h, and the phase difference, ψ. The maximum thrust efficiency found experimentally was 87%[2]. Taylor[5] pointed out that the *St* of flapping wings or tails is maintained within a narrow range during flying or swimming. Rohr[6] discovered that the *St* of swimming dolphins is within the range of 0.2~0.3, even at high cruising speeds. Techet[7] collected water tunnel data using a foil actuator module based on aquatic penguin or turtle fins, and found a maximum thrust coefficient of 2.09 and a thrust efficiency of over 70% in the *St* range of 0~0.6. The Reynolds number (*Re*) has little effect on the optimal thrust zone where *Re* lies between 20000 and

Corresponding author: Li Wen
E-mail: alex.wenli@gmail.com

50 000, and the preferred *St* of swimming fish is between 0.2 and 0.4[8]. By analyzing both biology research and control theory, we can consider that fish swim using reasonable vorticity control mechanisms, and thus achieve their desired swimming speed.

Through bionic engineering, the high thrust performance of fish can be adapted to make up for the defects in traditional underwater vehicle, such as low efficiency or poor maneuverability. The study of robotic fish has experienced rapid development since 1990. Draper researched thrust mechanisms, and obtained a maximum speed of 1.25 $m \cdot s^{-1}$ with the Vorticity Control Unmanned Underwater Vehicle (VCUUV)[9]. Kato *et al*. made "Blackbass" to study the thrust mechanism of pectoral fins[10]. Liang *et al*. utilized a biomimetic robotic fish for archeological detection[11]. Wen *et al*. demonstrated a robotic fish capable of long voyages; it operated for 7 hours over a distance of 22 km, with an average speed of 1.03 $m \cdot s^{-1}$ and a length-specific speed of 0.75[12]. Regarding control algorithms, Kato[13] achieved maneuverability and stability of pectoral fin propulsive robotic fish in 2D planar motion using fuzzy control. Yu[14] achieved 2D planar maneuverability of a carangiform swimming mode with an intelligent algorithm. Menozzi[15] presented an open-loop control system for a multi-fin biomimetic rigid-hull underwater vehicle, which resulted in good maneuvering performance. This control system, based on cycle-averaged experimental data, was used to analyze the hydrodynamic forces produced by a single foil as a function of its kinematic motion parameters. Indeed, the hydrodynamic model for swimming fish is complicated. Current robotic fish motion control research mainly focused on open-loop swimming gait generation and hydrodynamic model-based control. The open-loop swimming gait generation method used discrete joint movement to fit the continuous undulating body curve[16], as well as CPG control method[17]. Model-based control generally used analytical methods based on quasi-steady assumptions and added mass unsteady fluid effect, thus, trajectory tracking as well as maneuvering control simulation could be carried out[18]. In practice, most analytical methods for robot fish were based on slender body theory[19] and its improved form[20], however, the computational accuracy of this method is poor when the waving amplitude of the tail fin or the thickness of the body are large. Numerical CFD can produce relatively high-precision results, but solution of the real-time problem is a major deficiency. Rule-based motion control could resolve the non-model problem to some extent[10,14], however, the hydrodynamic experiment result was very difficult to obtain. Actually the robotic fish thrust performance consists of two main aspects: swimming speed (or angular speed) and thrust efficiency. Although direct motion control can achieve the control objectives, the thrust efficiency during swimming cannot be assured. Considering the flow physics, direct control based on motion parameters cannot obtain optimal vortex wake patterns for biologically inspired robots.

Methods for achieving high thrust efficiency during steady swimming of biomimetic robotic fish are of great significance. Reversed Karman vortex is a typical shedding mode for fish[3], and the vorticity control parameters have important effects on the vorticity pattern by a swimming fish[21]. Consequently, thrust performance could be affected by the vorticity control parameters[8]. This paper discusses a method to achieve high efficiency swimming using "fuzzy logic vorticity control" with a flapping tail. Field tests of biomimetic robotic fish verify the control methods.

2 Materials and methods

2.1 Oscillating foil kinematics and hydrodynamic experiments

Hydrodynamic experiments were conducted in a horizontal low-velocity water tunnel to ascertain the thrust efficiency and thrust coefficient of the flapping lunate tail in free stream conditions. This water tunnel has been used previously for dragonfly flapping wing and biomimetic robotic fish flow visualization[22,23]. The water tunnel has a running speed range of 0.05 to 1 $m \cdot s^{-1}$, and the uniformity of the flow velocity is 0.2%. The flapping foil has two degrees of freedom: transverse and rotational. Forces are measured on a flat-plate lunate tail fin, which has a span of 350 mm, chord of 70 mm, aspect ratio of 5, lunate tail sweepback angle of 70°, and thickness of 3 mm.

The transverse and rotational motions of the flapping tail are defined as

$$h'(t) = h_f \times \sin(2\pi f t) \ , \tag{1}$$

$$\theta(t) = \theta_f \times \sin(2\pi f t + \psi) \ , \tag{2}$$

where h_f represents the amplitude of transverse motion, f

represents the flapping frequency, θ_f represents the amplitude of rotation, and ψ is defined as the phase angle between transverse and rotational motion.

As shown in Fig. 1, the tail flaps transversely by means of mechanical links that describe an arc. When the length of the link staff l is large and the angle θ_f is relatively small, the length of the arc is approximately equivalent to the transverse displacement. In this experiment, l = 0.36 m and $\theta_f < 15^\circ$, which satisfies this approximation. If we suppose that A represents the angular amplitude (in radians) of the transverse motion, the transverse tail kinematic trajectory $H(t)$ can be defined as

$$H(t) = l\sin\theta_h \approx l\theta_h = lA\sin(2\pi ft) = h_f\sin(2\pi ft)\,. \quad (3)$$

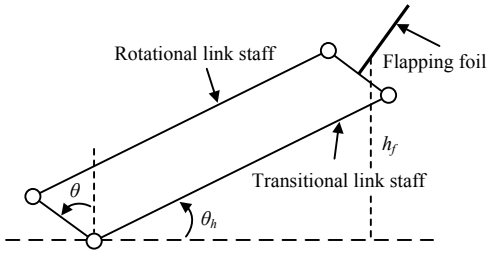

Fig. 1 Tail fin flapping mechanism.

After considering the relationship between the flapping tail kinematics and the vorticity control, we define *St* based on chord length as

$$St = \frac{2fh_f}{U} = \frac{2fAl}{U}, \quad (4)$$

where h_f is the transverse amplitude, and U is the incoming flow velocity. It can be seen from Fig. 2 that the tail's transverse motion is along the direction of the dh/dt axis. The velocity of the incoming flow is perpendicular to the transverse motion, which leads to the following equation:

$$\tan(\alpha(t) + \theta(t)) = (\mathrm{d}h/\mathrm{d}t)/U\ . \quad (5)$$

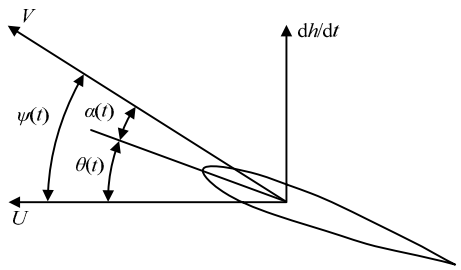

Fig. 2 Definition of relative velocity V and angle of attack $\alpha(t)$ for a flapping tail.

Taking Eqs. (3) and (5) into consideration, the angle of attack of flapping tail, $\alpha(t)$, can be defined as

$$\alpha(t) = \arctan\left(\frac{2\pi flA\cos(2\pi ft)}{U}\right) - \theta_f \times \sin(2\pi ft + \psi)\,. \quad (6)$$

The maximum value of $\alpha(t)$ is $\alpha_{\max}$, which is an important derived parameter in describing the performance of a flapping tail. The term $\alpha_{\max}$ has a large influence on the leading-edge vorticity, and thus a significant impact on the thrust efficiency[2]. The dimensionless transverse motion amplitude, h, is defined as

$$h = h_f / c\,, \quad (7)$$

where c is the chord length of the lunate tail.

We performed systematic tests at several fixed non-dimensional transverse motion amplitudes, with settings matching those of previous experiments on 2D and 3D flapping foils[7]. The amplitude h was set to a range of values (h = [0.75, 1.0, 1.5]), and at each value of h the tests were performed for several angles of attack: $\alpha_{\max}$ = [5°, 15°, 25°, 35°]. For each combination of h and $\alpha_{\max}$, *St* was varied systematically from 0.08 to 0.60 in small increments. The flapping frequency was 0.4 to 2.5 Hz for the actual flapping mechanism, which determines the range of *St*. The phase angle was specified as $\psi = 90^\circ$ for all experiments.

Re based on chord length is defined as

$$Re = \frac{U \times c}{\nu}, \quad (8)$$

where ν is the kinematic viscosity of the fluid. The experiments were conducted under the following conditions: the temperature during force and power measurements was approximately 15 to 20 °C, $\nu = 10^{-6}$ m^2·s^{-1}, Re = 20 000, and U = 0.28 m·s^{-1}.

The motion control parameters of the flapping tail are A, θ_f, f, ψ, whereas *St*, $\alpha_{\max}$, h, ψ represent the vorticity control parameters that determine thrust performance. The relationships between vorticity control and motion control parameters are given in Eqs. (4) to (7).

The mean thrust coefficient, C_t, is defined as:

$$C_t = \frac{\int_0^T F_x \mathrm{d}t}{(0.5\rho U^2 cS)}\ , \quad (9)$$

where ρ is the fluid density, S is the span length, F_x represents the measured thrust, and T is the flapping period.

The thrust efficiency, η, is defined as the useful power output divided by the power input

$$\eta = \frac{\frac{1}{T}\int_0^T F_x \mathrm{d}t \times U}{\frac{1}{T}(\int_0^T (M_t \times \omega_t)\mathrm{d}t + \int_0^T (M_r \times \omega_r)\mathrm{d}t)}, \quad (10)$$

where M_t is the measured torque of the transverse motion and ω_t is the corresponding angular velocity. Likewise, M_r is the measured torque of the rotational motion and ω_r is the corresponding angular velocity.

Experiments were conducted (see Fig. 3) using two servo motors (maxon RE40, 150w) symmetrically assembled, coupled with a reducer in order to provide larger torque. Meanwhile the flapping mechanism (see Fig. 2) simulates caudal fin movement in the water channel, motion coordinator and Trio MC206 and motor amplifier will be used to ensure that the motion curve of the caudal fin model is accurate. The dynamic force and moment vectors [F_x, M_t, M_r] were measured in the experiment: F_x was measured by a 25 kg Kislter single-component pressure sensor, and M_t, M_r, ω_t, and ω_r were measured by a dynamic torque sensor connected at the root of the output axis (see Fig. 4) (note that this torque sensor can measure both torque and the angular velocity). Unlike the heave and pitch foil motion in Anderson's experiment[2], the span-wise direction of the tail fin is perpendicular to the coming flow direction in current experiment. The upper border of the tail fin is 200 mm below the water surface to minimize interference of free water surface. We used Nicolet VisionXP as the data acquisition and recording device, which has 16 sample channels and a maximum sampling rate of 100 kHz.

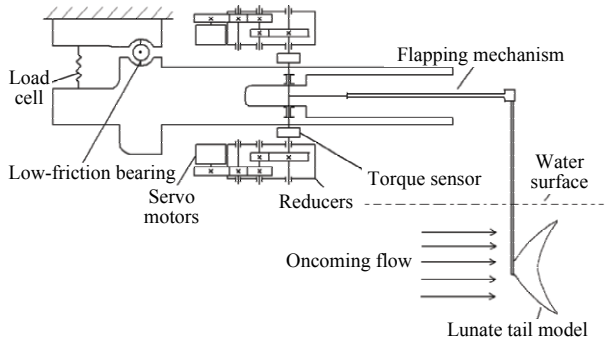

Fig. 3 Apparatus used for conducting flapping foil force and power measurement.

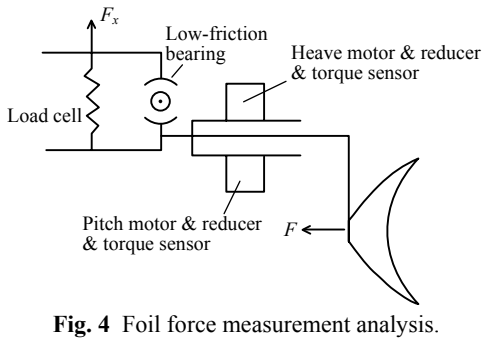

Fig. 4 Foil force measurement analysis.

The purpose of the experiment is to measure the unsteady fluid force and torque produced by the flapping foil in water. The total force includes the hydrodynamic force from fluid effects, the inertia force of the flapping mechanism and the initial force caused by preload and the mass of the model. The latter two forces could be measured as follows: first remove the caudal fin model, replace it with a steel tube of diameter 3 mm and length 350 mm (the same mass with tail model) so as to produce less aerodynamic force than the large area tail, record the force and torque at different vorticity control parameters. Unsteady fluid force and torque could then be derived by removing the latter two sources of force from the total force.

The terms C_t and η are used to quantify the thrust of the flapping lunate tail. A regional division of the thrust performance as a function of *St* regulated vorticity control. By varying h, the thrust performance can be divided into multiple thrust modes. The force measurements from over 200 experiments are shown in Fig. 5. The general trend of the thrust force results showed similarities with those for the 2D case[2]. When $\alpha_{max} = 5^\circ$, the thrust coefficient is small for all values of *St*, and even a

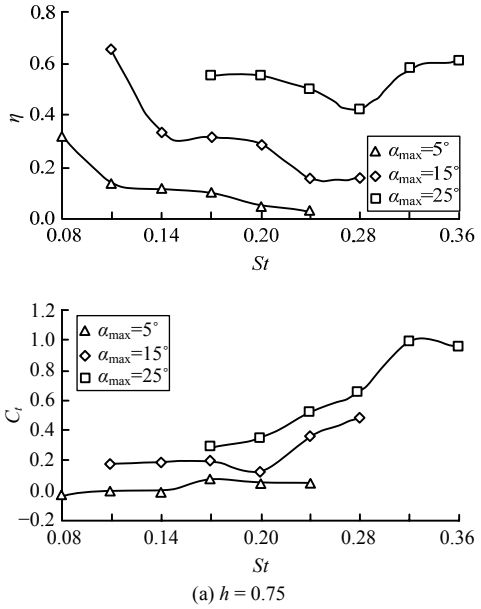

(a) h = 0.75

Fig. 5 Plots of thrust coefficient C_t and efficiency η for different h = 0.75, 1.0, and 1.5 as function of *St* and α_{max}, respectively.

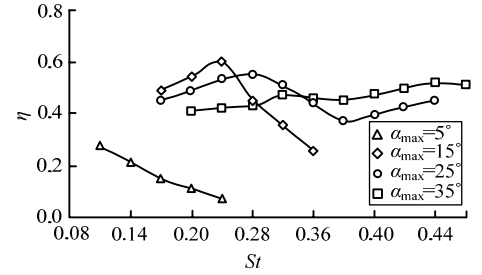

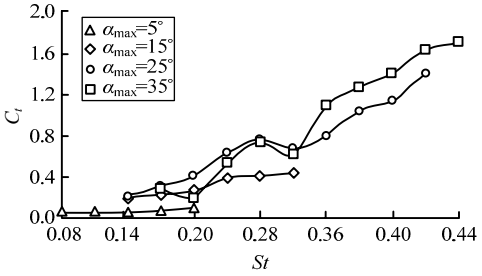

(b) h = 1.00

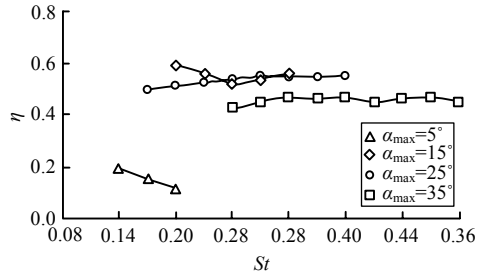

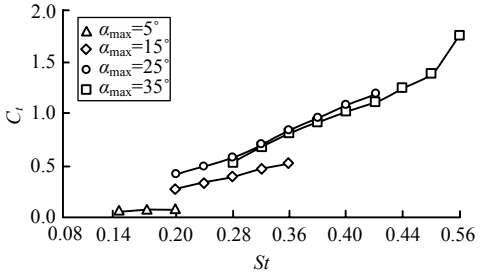

(c) h = 1.50

Fig. 5 Continued.

negative value appeared (at h = 0.75). It can therefore be inferred that a small angle of attack produces poor thrust. At a non-dimensional amplitude of 0.75 (h = 0.75), a peak thrust coefficient of 0.99 is recorded at St = 0.32, α_{max} = 25°, and the highest thrust efficiency recorded is about 0.65, centered on St = 0.16, α_{max} = 15°. While at h = 1.0, the peak thrust coefficient is 1.71 recorded at St = 0.45, α_{max} = 35°, and at St = 0.28, α_{max} = 25°, the peak thrust efficiency was record η = 0.55.When extrapolating to h = 1.5, a higher peak thrust coefficient of C_t = 1.75 could be achieved at St = 0.56, α_{max} = 35°, and maximum thrust efficiency of η = 0.56 appeared at St = 0.36, α_{max} = 15°. To sum up, the thrust coefficient increases with St and α_{max}. However, the changes of thrust efficiency have a more complex relationship with St and α_{max} at different non-dimensional amplitude. The highest thrust efficiency and maximum coefficient could not be produced at the same St, and do not even share the trend with the function of St. With increasing St, thrust performance would first reach the highest thrust efficiency location point then achieve the maximum thrust coefficient later. The largest St considered in the current experiments was 0.56. One could speculate that a higher thrust coefficient could be achieved on extrapolation of the St. A similar increase was found in the experiment on thrust of a 3D flapping rigid foil at relatively high Re by Techet[7]. While for a given St thrust efficiency would increase with dimensionless amplitude h, there was no significant change in thrust coefficient. In other words, at the same St, better thrust could obtain at larger dimensionless amplitude. This agrees with Read's study on a finite 2D flapping foil[4].

Zonal division of thrust as a function of St was considered for vorticity control. By varying h, the thrust performance can be divided into multiple thrust modes based on the force measurement result discussed above. We summed up the hydrodynamic results in Eqs (11) to (13):

$$\alpha_{max}=\begin{cases}5^\circ\ (0.08\le St\le 0.14, h=0.75)\ \text{mode}1\\ 15^\circ\ (0.14\le St\le 0.22, h=0.75)\ \text{mode}2\\ 25^\circ\ (0.22\le St\le 0.36, h=0.75)\ \text{mode}3\end{cases}, \quad (11)$$

$$\alpha_{max}=\begin{cases}5^\circ\ (0.08\le St\le 0.14, h=1.0)\ \text{mode}1\\ 15^\circ\ (0.14\le St\le 0.25, h=1.0)\ \text{mode}2\\ 25^\circ\ (0.25\le St\le 0.35, h=1.0)\ \text{mode}3\\ 35^\circ\ (0.35\le St\le 0.45, h=1.0)\ \text{mode}4\end{cases}, \quad (12)$$

$$\alpha_{max}=\begin{cases}5^\circ\ (0.14\le St\le 0.2, h=1.5)\ \text{mode}1\\ 15^\circ\ (0.2\le St\le 0.25, h=1.5)\ \text{mode}2\\ 25^\circ\ (0.25\le St\le 0.4, h=1.5)\ \text{mode}3\\ 35^\circ\ (0.45\le St\le 0.6, h=1.5)\ \text{mode}4\end{cases}. \quad (13)$$

As shown in Eqs. (11) to (13), when h = 0.75, the mode 1 thrust range is 0 < St < 0.14, α_{max} = 5°, and C_t is very low in this region. Low values of C_t can even produce negative thrust if accompanied by low efficiency (0.25 < η < 0.35). The mode 2 thrust range is 0.14 < St < 0.22, and for α_{max} = 15°, both C_t and η are higher than the other cases (i.e. when St < 0.22, the mechanism

cannot generate a larger α_{max}). The maximum *St* used in the experiments (restricted by the amplitude and frequency of the mechanism) were 0.45 and 0.56 with h = 1.0 and h = 1.5, respectively. With h = 1.0, C_t and η in thrust mode 1 were both low, while thrust mode 2 gave low C_t and high η. Relatively high C_t and η were found in thrust mode 3. The C_t in thrust mode 4 was high but η decreased slightly compared with the values in modes 2 and 3. Overall, the thrust modes with h = 1.5 and h = 1.0 were similar. Anyway, Eqs. (11) to (13) can be treated as summary of the force measurement result in Fig. 5.

Methods for achieving relatively high swimming efficiency and improving the thrust performance of biomimetic robotic fish are significant. Trantyfyllou[3] observed fish during high efficiency swimming phases and discovered that the corresponding *St* ranged between 0.2 and 0.4. However, the differences in drag and thrust performance between biomimetic robotic fish and live fish caused the biomimetic machine to lag behind the live animal in both speed and efficiency. Previous researchers have described the thrust performance of flapping aquatic animals with *St*, *Re*, and length-specific swimming speed. Therefore, it is necessary to discuss whether biomimetic vehicles can achieve the maximum ability of tail fin thrust by reasonable vorticity control methods.

2.2 Biomimetic robotic fish with lunate flapping tail

The biomimetic fish "SPC" is cylindrical, with diameter of 0.22 m, length of 1.6 m, and an oscillating foil thrust cabin located behind the main body (Fig. 6). Note that the thrust cabin displacement is only 10% of the entire body. The battery, sensors, and other electronics make up 70% of the displacement. The power supply uses 26 lithium polymer batteries. Two 150 W DC servomotors with reducers were installed symmetrically in the thrust cabin, with two concentric output axes directly driving a connecting rod to provide the transverse and rotational movements to the flapping tail. The tail is made of carbon fiber, with a chord of 10 cm, a span of 50 cm, and a sweepback angle of 70°. The transverse and rotational motions are coordinated by a Trio MC206 motion controller. The maximum flapping frequency of the foil is 2.5 Hz, based on mechanical system tests. An HMR3100 compass and an ADXRS150 gyro were installed in SPC, and depth control was achieved with an FMP200 pressure sensor and a pair of elevators.

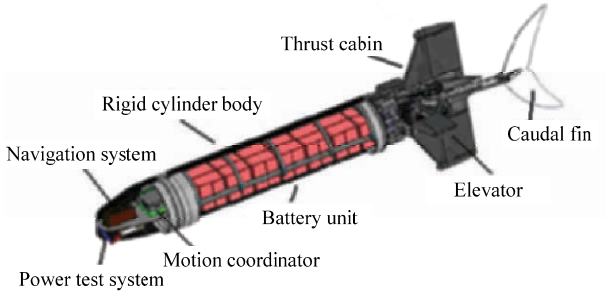

Fig. 6 View of SPC-3 UUV layout.

The velocity feedback is obtained from a modified LS10 flow kinemometer fixed under the head of SPC. When water current acts on the blades of the kinemometer it produces a rotational motion, measured by waterproof photoelectric encoders. Static and dynamic calibration determined the relation between flow velocity V and rotational speed n. Static calibration consisted of fixing the flow kinemometer to a guide rail and moving the sensor at uniform velocities. A least-squares data fitting procedure yielded the linear relation $V = 0.0998n + 0.037$, with a mean square deviation of 1.64%. The dynamic calibration consisted of applying acceleration-deceleration to a preset guide rail movement. The mean square deviation of the guide rail velocity preset is 2.2% in the range of 0.08 to 2.1 $m \cdot s^{-1}$.

The onboard encoder signal is converted to an analog signal via a frequency-voltage converting device, then processed by the Trio MC206. Two Honeywell CS050 current indicators measure the input currents I_1 and I_2 of the two servo motors. These currents, in addition to the battery voltage V obtained from the PC104, allow the power consumption W of the robotic fish to be calculated with $W = (I_1 + I_2) \times V$. The power consumption includes the hydrodynamic power spent in the fluid and the inertial power spent on the flapping mechanism, system preload, mechanical friction loss, *etc*. Because the hydrodynamic power and speed are used to evaluate thrust, we need to isolate the hydrodynamic power from the other power types.

2.3 Fuzzy logic vorticity control methods

Conventional motion control cannot achieve efficient propulsion at a range of speeds. Vorticity control is rule-based with velocity feedback. Its main purpose is to establish the functional relationship between swimming velocity and *St*, after which the other vorticity control parameters α_{max}, h and ψ can be confirmed, resulting in

the thrust modes given in Eqs. (11) to (13). Thus, a Fuzzy Logic Vorticity Controller (FLVC) based on hydrodynamic experimentation can be built (see Fig. 7).

According to the velocity sensor feedback, the robotic fish first determines the thrust mode by taking the difference between the current and the target speeds. Then *St* and the rest of the vorticity control parameters of the tail are adjusted to match the target speed. As shown in Fig. 7, the input of the fuzzy vorticity control system is the velocity deviation *e* and the deviation rate of change *ec*, which contain the difference between the feedback velocity U' and the desired speed U_{set}. The control system outputs *St* after a defuzzification operation and chooses a suitable α_{max} from the resulting *St*. Vorticity control parameters *St*, α_{max}, ψ and *h* are determined such that the non-dimensional amplitude satisfies h = 0.75, 1.0, or 1.5, and $\psi = 90^{\circ}$. The required thrust state can then be determined according to Eqs. (11) to (13). It should be noted that it is impossible to convert between the vorticity control parameters *St*, α_{max}, ψ, *h* and the motion control parameters *f*, *A*, θ, ψ without velocity feedback (*U* in Fig. 7).

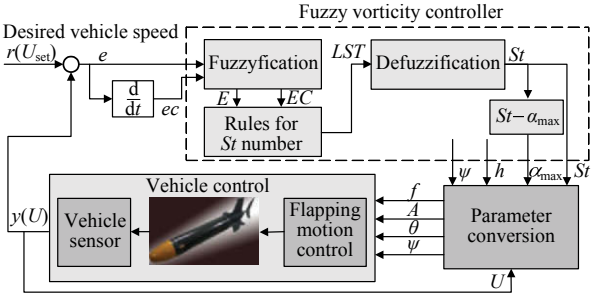

Fig. 7 Block diagram of SPC's fuzzy logic vorticity controller.

Given two control inputs *r* and *y*, where *r* ,*y* are the desired speed and velocity feedback, respectively, the *e* and *ec* at a certain instant are defined as $e_t = r_t - y_t$ and $ec_t = e_t - e_{t-1}$. In our experiments, these values were set to the ranges: $-2\ \text{m}\cdot\text{s}^{-1} \le e \le 2\ \text{m}\cdot\text{s}^{-1}$ and $-0.2\ \text{m}\cdot\text{s}^{-1} \le ec \le 0.2\ \text{m}\cdot\text{s}^{-1}$. A positive *e* means that the robotic fish is accelerating, whereas a negative value means the robot is decelerating. The output range of *St* is $0 < St < 0.6$, which is also the range tested in the hydrodynamic experiments. The terms *e*, *ec* and *St* are all divided into 13 levels, and after multiplying by scaling factors, the resulting range is – 6 to 6, i.e. {–6, –5, –4, –3, –2, –1, 0, 1, 2, 3, 4, 5, 6}. The domains of *e*, *ec*, and *St* after fuzzification by membership functions are expressed as *E*, *EC*, and *LST*, respectively. At the fuzzification stage, *E*, *EC* and *LST* are all divided into 7 levels, represented by three groups of linguistic fuzzy sets: NB (negative big), NM (negative medium), NS (negative small), ZE (zero), PS (positive small), PM (positive medium), and PB (positive big). Each membership function is expressed by a triangular function.

The fuzzy rule is constituted by a 7 × 7 fuzzy associative memory matrix (see Table 1). It adjusts the thrust mode of the tail fin using the velocity deviation and current acceleration. We use the following terms in the fuzzy rules: E_i is the *i*-th member of the fuzzy set *E*; EC_j is the *j*-th member of the fuzzy set *EC*; and b_{ij} denotes one of the members of the fuzzy set *LST*. The fuzzy rules are then defined as: if *E* is NB and *EC* is PS, then *LST* is PB; if *e* is E_i and *ec* is EC_j then *St* is b_{ij}. This fuzzy logic can be interpreted as follows: when the fish encounters a state of h = 1.5, $\psi = 90^{\circ}$, the difference between the target velocity and the current velocity is negative and large, and the vehicle's acceleration is positive but small, then the vehicle needs to accelerate to reach the desired target speed. Consequently, the tail fin *St* will be increased to produce a large thrust coefficient, generating the required acceleration (e.g. thrust mode 4 in Eq. (13). After the *LST* is obtained from the defuzzification stage, the method of center of gravity is used to get *St* required for precision control. $St - \alpha_{max}$ is an important transferring block, for the output of defuzzification is *St*. However, the optimal thrust performance of a flapping tail could be achieved only by adopting a proper combination of vorticity parameters *St*, α_{max}, ψ, *h*, where ψ, *h* are defined. The purpose of $St - \alpha_{max}$ is to choose the appropriate α_{max} so as to achieve the different thrust modes described in Eqs. (11) to (13). Thus high thrust efficiency of the flapping tail is obtained.

Table 1 Rule table for fuzzy vorticity control

LST		Charge-in-error *EC*						
		NB	NM	NS	ZE	PS	PM	PB
E	NB	NS	NS	PS	PB	PB	PB	PB
	NM	NS	NS	PS	PM	PB	PB	PB
	NS	NM	NS	PS	PM	PM	PB	PB
	ZE	NM	NS	NS	ZE	PS	PM	PB
	PS	NM	NS	NS	ZE	PS	PM	PM
	PM	NM	NM	NS	NS	PS	PS	PM
	PB	NB	NM	NS	NS	PS	PS	PM

After the vorticity control parameters (*St*, α_{max}, ψ, *h*) and the converted motion control parameters (*f*, *A*, ψ,

h) are acquired by the method described above, the tail fin vorticity controller is programmed into the Trio MC206 motion coordinator using BASIC language. The membership functions and the fuzzy control rules are both stored in the controller's flash memory. The vorticity control model is configured with a control cycle period of 0.5 s, i.e. every time a flapping cycle is completed, f, A, ψ, h are updated by the control algorithm. The target velocity of the robotic fish is set within $0.5 < U_{set} < 2.0$ because the current vorticity control algorithm cannot be used for acceleration from a stationary position (i.e. the St velocity defined previously is meaningless when the vehicle speed is zero).

3 Results

It is necessary to acquire St and thrust power consumption at varying swimming speeds to verify if the vorticity controller can achieve a higher speed and thrust efficiency than a direct motion control method. The power experiments here must subtract the effects of the tail fin flapping in the air, similar to the hydrodynamic experiment.

A free-swimming field test was conducted in a swimming pool 25 m wide, 1.5 m deep, and 50 m long. The SPC inertial navigation system and sensors were calibrated prior to the experiments. Because the vorticity control algorithm cannot be used at $U = 0$, a 1 Hz flapping frequency is first commanded to the tail to accelerate the robotic fish to a speed of 0.5 m·s^{-1}, then the vorticity control algorithm is activated. The vehicle performance was compared under the vorticity control algorithm and normal motion control at different non-dimensional transverse amplitudes (h/c = 0.75, 1.0, 1.5). The maximum flapping frequency of the mechanism was limited to 2.5 Hz. The vorticity control algorithm causes the fish to accelerate gradually from 0.5 m·s^{-1} to the target speed, initially set to 1.4 m·s^{-1}.

As shown in Fig. 8, when the motion control was used with h = 1.5, the maximum speed was 1.4 m·s^{-1} at 2.5 Hz. When vorticity control was used, the maximum speed was 1.87 m·s^{-1}, where the speed was fed back via the kinemometer. This shows that under vorticity control less energy is used than with the direct motion frequency controller for the same h. For example, the vorticity controller with h = 0.75 and v = 0.7 m·s^{-1} consumed 3 W less than the corresponding motion controller. The experiments also showed that at a speed of 1.4 m·s^{-1}, the vorticity controller flapping frequency was 2.0 Hz, whereas the direct frequency controller reached 2.5 Hz. Among the three non-dimensional transverse amplitudes (h = 0.75, 1.0, 1.5) tested with the vorticity control, as h increases, the power consumption decreases. Likewise, the highest thrust efficiency from this group occurred at h = 1.5. This is consistent with the experimental results of Ref. [4], which indicated that at a constant St, large-amplitude low-frequency flapping produces higher thrust than low-amplitude high-frequency flapping. At the same St a larger h produces a higher speed (i.e. at h = 1.0 the maximum speed is 1.6 m·s^{-1}, but at h = 1.5 the maximum speed is 1.87 m·s^{-1}).

The relation between St and maximum steady swimming speed for both control methods is shown in Fig. 9. The St varies from 0.59 to 0.64 under direct motion control (with the flapping frequency reaching 2.5 Hz), whereas the it varies from 0.42 to 0.5 under vorticity control. Thus, fuzzy vorticity control controls St actively. Fig. 9 shows that when St is controlled within a reasonable range, high thrust efficiency can be obtained. It could be inferred that vorticity control is a biology-inspired method to acquire better vehicle thrust performance than the conventional motion control methods.

Within a steady speed range of 0.5~1.87 m·s^{-1}, the

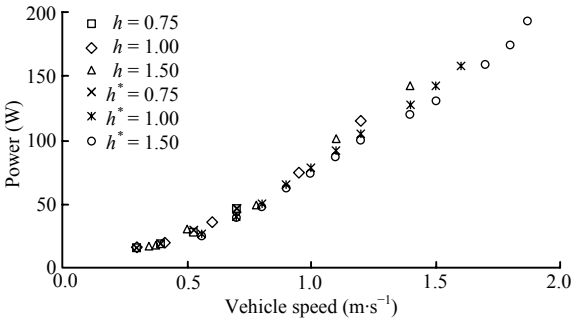

Fig. 8 Robotic fish speed vs. power consumption under motion control and vorticity control.

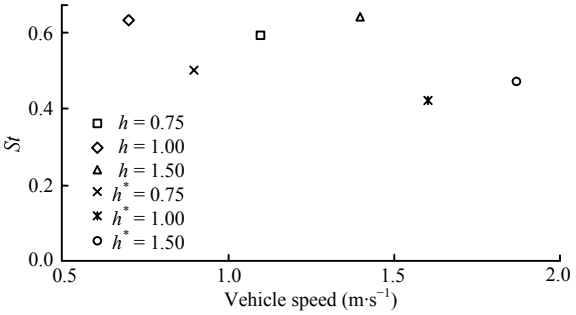

Fig. 9 Maximum swimming velocity versus St as a function of different control methods

robotic fish with vorticity control achieves *St* in the range of 0.4~0.5, but the observed range of *St* for cruising aquatic animals is 0.2~0.4. The robotic fish produces a higher *St* than biological systems, providing evidence that a gap exists between the thrust efficiency of bionic machines and biology.

Table 2 compares the cruising *Re* and *St* of a variety of fish and our biomimetic robotic fish. The fish vary *St* by moving their tail fins and swimming at different speeds; their *St* generally does not exceed 0.4, but they reach higher length-specific speeds than SPC. The disparity between SPC and live fish comes from two sources: body drag and the tail fin thrust. Because SPC has a rigid cylindrical body, it has fewer skin friction or drag reduction mechanisms than live fish. Barrett[24] made a detailed study of drag reduction mechanisms and emphasized the effects of a laminar boundary layer and caudal fin vorticity control on the thrust performance. Thus, *St* encapsulates body drag and the tail fin's thrust ability for a steady-swimming biomimetic fish.

Table 2 *Re*, *St* and length-specific swimming speed for SPC and a variety of fish

Genera	Observed *St*	Maximum length-specific swimming speed	*Re*
Mackerel*	0.30	6.1	1×10^6
Dolphin*	0.28~0.30	3.5	8×10^5
Shark*	0.25~0.27	1.86	6×10^5
Saithe**	0.18	3.0	6×10^3
Goldfish*	0.30~0.35	6.3	8×10^4
Cod**	0.25 ~0.35	1.9	4×10^4
Rainbow Trout*	0.25~0.38	2.1	2.5×10^4
SPC	0.4~0.5	1.17	2×10^5

Where data marked with * come from Ref. [3], and ** come from Ref. [16]

As shown in the SPC swimming experiments, as speed increases (i.e. as *Re* increases), *St* decreases slightly. Read[4] found the same in the study of 2D flapping foils. Borazjani[25] reported in a study of carangiform swimming that for a given *St*, an increase in *Re* enhances the thrust efficiency. The relation between *Re* and *St* and their effect on vorticity control will be dealt with in future work.

In addition to the swimming pool tests, the SPC was used for water-quality testing experiments in Taihu Lake (see Fig. 10). It carried a water-quality testing instrument over a 50.79 km voyage, achieving an endurance time of 11.7 hours. Thus, the biomimetic robotic fish made its contribution to environmental monitoring.

Fig. 10 SPC swimming in Taihu lake.

4 Discussion

This article proposed a FLVC via velocity feedback to provide improved vehicle speed and power consumption. Because the flapping foil mechanism is considered a basic model for biomimetic thrust kinematics and dynamics, this control method can also provide an effective high-efficiency thrust mechanism for pectoral fin swimming and flapping and hovering flight. Although fish swim accompanied by lateral and rotation movement, however, they are relatively small compared with the forward speed, so predecessors always chose to basically ignore the effect in these two directions, focusing on thrust while studying steady swimming[8]. As dorsal and anal fins were used to enhance the robotic fish's stability so we decided to ignore the lateral and rotation movement in our studies. Thus the "vorticity control" proposed in this paper refers specifically to forward direction control.

A major goal of biomimetic robotic fish research is to obtain high thrust efficiently. Although the maximum swimming speed achieved by SPC in this study was 1.17 length specific speed, a higher speed may be achieved by: enhancing the power and strength of the mechanical parts; increasing the fluke area; appropriately increasing the flapping frequency, *etc*. But as the vehicle differs lot from live fish in drag, body-tail interaction, and caudal fin thrust efficiency, it becomes more difficult to decrease *St*. In these cases, it becomes more difficult to acquire a fish-like high thrust efficiency. The two basic requirements for improving biomimetic vehicles are reasonable tail fin vorticity control methods and impedance match of body drag and caudal fin thrust. Although the *St* for SPC now ranges from 0.42 to 0.5, we should consider lowering this number while still using vorticity control.

Acknowledgement

The authors are grateful to Prof. Hui Guo for his valuable insights throughout this project, Jinlan Li and

Zhe Fan for their assistance during the hydrodynamic experiment in the wet, hot water tunnel as well as field tests in swimming pool and Taihu lake. This work was supported in part by the National Outstanding Youth Science Foundation support projects, China (Contract No. 60525314), and the China Postdoctoral Science Foundation (No. 200902102).

References

[1] Triantafyllou M S, Triantafyllou G S, Yue D K P. Hydrodynamics of fishlike swimming. *Annual Review of Fluid Mechanics*, 2000, **32**, 33–53.

[2] Anderson J M, Streitlien K, Barrett D S, Triantafyllou M S. Oscillating foils of high propulsive efficiency. *Journal of Fluid Mechanics*, 1998, **360**, 41–72.

[3] Triantafyllou M S, Triantafyllou G S, Gopalkrishnan R. Wake mechanics for thrust generation in oscillating foils. *Physics of Fluids A*: *Fluid Dynamics*, 1991, **3**, 2835–2837.

[4] Read D A, Hover F S, Triantafyllou M S. Forces on oscillating foils for propulsion and maneuvering. *Journal of Fluids and Structures*, 2003, **17**, 163–183.

[5] Taylor G K, Nudds R L, Thomas A L R. Flying and swimming animals cruise at a Strouhal number tuned for high power efficiency. *Nature*, 2003, **425**, 707–711.

[6] Rohr J J, Fish F E. Strouhal numbers and optimization of swimming by odontocete cetaceans. *The Journal of Experimental Biology*, 2006, **207**, 1633–1642.

[7] Techet A H. Propulsive performance of biologically inspired flapping foils at high Reynolds numbers. *The Journal of Experimental Biology* , 2008, **211**, 274–279.

[8] Triantafyllou M S, Hover F S, Techet A H, Yue D K P. Review of hydrodynamic scaling laws in aquatic locomotion and fishlike swimming. *Applied Mechanics Reviews*, 2005, **58**, 226–236.

[9] Anderson J M, Chhabra N K. Maneuvering and stability performance of a robotic tuna. *Integrative and Comparative Biology*, 2002, **42**, 118–126.

[10] Kato N. Control performance in the horizontal plane of a fish robot with mechanical pectoral fins. *IEEE Journal of Oceanic Engineering*, 2000, **25**, 121–129.

[11] Liang J. Propulsive Mechanism of Bionic Undersea Vehicle. Doctoral Thesis, Beijing University of Aeronautics and Astronautics, Beijing, 2006. (in Chinese)

[12] Wen L, Liang J, Wang T, Song Y. Experimental design and performance of underwater vehicle based on capacity of voyage. *Journal of Beijing University of Aeronautic and Astronautics*, 2008, **34**, 340–343.

[13] KatoN, Liu H, Morikawa H. *Proceedings of* 12*th International Offshore and Polar Engineering Conference*, 2002, **2**, 269–276.

[14] Yu J, Tan M, Wang S, Chen E. Development of a biomimetic robotic fish and its control algorithm. *IEEE Transactions on Systems*, *Man and Cybernetics*, *Part B*: *Cybernetics*, 2004, **34**, 1798–1810.

[15] Menozzi A, Leinhos H A, Beal D N, Bandyopadhyay P R. Open-loop control of a multifin biorobotic rigid underwater vehicle. *IEEE Journal of Oceanic Engineering*, 2008, **33**, 59–67.

[16] Yu J, Wang L. Parameter optimization of simplified propulsive model for biomimetic robot fish. *Proceedings of the IEEE International Conference on Robotics and Automation*, Barcelona, Spain, 2005, 3317–3322.

[17] Zhao W, Hu Y, Zhang L, Wang L. Design and CPG-based control of biomimetic robotic fish. *IET Control Theory and Applications*, 2009, **3**, 281–293.

[18] Saimek S, Li P Y. Motion planning and control of a swimming machine. *The International Journal of Robotics Research*, 2004, **23**, 27–53.

[19] Lighthill M J. Note on the swimming of slender fish. *Journal of Fluid Mechanics*, 1960, **9**, 305–317.

[20] Lighthill M J. Aquatic animal propulsion of high hydromechanical efficiency. *Journal of Fluid Mechanics*, 1970, **44**, 265–301.

[21] Wolfgang M J, Anderson J M, Grosenbaugh M A, Yue D K, Triantafyllou M S. Near-body flow dynamics in swimming fish. *The Journal of Experimental Biology*, 1999, **202**, 2303–2327.

[22] Tan G K, Shen G X, Huang S Q, Su W H, Yu K. Investigation of flow mechanism of a robot fish swimming by utilising flow visualization synchronized with hydrodynamic force measurement. *Experiments in Fluids*, 2007, **43**, 811–821.

[23] Lu Y, Shen G X, Lai G J. Dual leading-edge vortices on flapping wings. *The Journal of Experimental Biology*, 2006, **209**, 5005–5016.

[24] Barrett D S, Triantafyllou M S, Yue D K P, Grosenbaugh M A, Wolfgang M J. Drag reduction in fish-like locomotion. *Journal of Fluid Mechanics*, 1999, **392**, 183–212.

[25] Borazjani I, Sotiropoulos F. Numerical investigation of the hydrodynamics of carangiform swimming in the transitional and inertial flow regimes. *The Journal of Experimental Biology*, 2008, **211**, 1541–1558.